JOURNAL OF SPACECRAFT AND ROCKETS
Vol. 43, No. 2, March–April 2006

Experimental Hypersonic Aerodynamic Characteristics of Mars Surveyor 2001 Precision Lander with Flap

Thomas J. Horvath,* Tod F. O'Connell,† F. McNeil Cheatwood,‡ Ramadas K. Prabhu,§ and Stephen J. Alter*
NASA Langley Research Center, Hampton, Virginia 23681

Aerodynamic wind-tunnel screening tests were conducted on a 0.029-scale model of a proposed Mars Surveyor 2001 Precision Lander (70-deg half-angle spherically blunted cone with a conical afterbody). The primary experimental objective was to determine the effectiveness of a single flap to trim the vehicle at incidence during a lifting hypersonic planetary entry. The laminar force and moment data, presented in the form of coefficients, and shock patterns from schlieren photography were obtained in the facilities of the NASA Langley Aerothermodynamic Laboratory for postnormal shock Reynolds numbers (based on forebody diameter) ranging from 2.637×10^3 to 92.35×10^3, angles of attack ranging from 0 up to 23 deg at 0- and 2-deg sideslip, and normal-shock density ratios of 5 and 12. Based upon the proposed entry trajectory of the 2001 Lander, tests in the heavy gas CF_4 simulate a Mach number of approximately 12 based upon a normal shock density ratio of 12 in flight at Mars. The results from this experimental study suggest that when the traditional means of providing aerodynamic trim for this class of planetary entry vehicle are not possible (e.g., offset c.g.), a single flap can provide similar aerodynamic performance. An assessment of blunt-body aerodynamic effects attributed to a real gas was obtained by synergistic testing in Mach 6 ideal air at a comparable Reynolds number. From an aerodynamic perspective, an appropriately sized flap was found to provide sufficient trim capability at the desired lift-to-drag ratio for precision landing. Inviscid hypersonic flow computations using an unstructured grid were made to provide an assessment of the viability of a flap to provide aerodynamic trim to the Lander. Subsequent Navier–Stokes computational predictions were found to be in very good agreement with experimental measurement.

Nomenclature

b_{REF}	=	reference span of model, in.
C_A	=	axial-force coefficient, axial-force/$q_\infty S_{REF}$
C_l	=	rolling-moment coefficient rolling-moment/$q_\infty S_{REF} b_{REF}$
$C_{l,\beta}$	=	$\Delta C_l/\Delta\beta$, per degree
C_m	=	pitching-moment coefficient, pitching-moment/$q_\infty S_{REF} L_{REF}$
C_N	=	normal-force coefficient, normal-force/$q_\infty S_{REF}$
C_n	=	yawing-moment coefficient, yawing force/$q_\infty S_{REF}$
$C_{n,\beta}$	=	$\Delta C_n/\Delta\beta$, per degree
C_Y	=	side-force coefficient, side-force/$q_\infty S_{REF}$
$C_{Y,\beta}$	=	$\Delta C_Y/\Delta\beta$, per degree
D	=	model base diameter, in.
L_{REF}	=	reference length, in.
M	=	Mach number
P	=	pressure, psi
q	=	dynamic pressure, psi
Re	=	Reynolds number
r	=	radius, in.
S_{REF}	=	model base reference area, in.^{2}
T	=	temperature, °R
$X_{c.g.}$	=	c.g. location
α	=	angle of attack, deg
γ	=	ratio of specific heats
θ	=	angle, deg
ρ	=	density, lbm/in^3

Subscripts

n	=	model nose
s	=	surface quantity or model support sting
sh	=	forebody shoulder
t, 1	=	reservoir conditions
w	=	wall
β	=	sideslip angle, deg
2	=	stagnation conditions behind normal shock
∞	=	freestream conditions

Introduction

THE next generation of Mars landers is being developed by NASA to provide a precision landing capability to within approximately 6 km of the targeted site.[1] This order-of-magnitude improvement in the accuracy associated with the targeted landing area will potentially enhance hazardous avoidance capability and allow geologically exciting (e.g., ice deposits recently detected beneath the surface of Mars by the orbiting Mars Odyssey spacecraft) or difficult-to-reach sites to be exploited by unmanned rovers for their scientific value. The demonstration of a precision landing would also represent a technology milestone towards the human exploration of Mars, where crewed expeditions will likely require advanced placement of cargo carriers and habitat modules within several hundred feet of each other.

The Mars Surveyor 2001 Precision Lander[2] (MSPL) was originally part of NASA's 10-year Mars Surveyor Program that was initiated in 1994. A precision landing demonstration by the lander was to have been accomplished through the use of advanced approach navigation techniques coupled with an actively controlled descent into the planetary atmosphere via a vehicle with a moderate lift-to-drag capability. As the result of a restructured[3–5] strategy for the exploration of Mars, the planned precision landing demonstration by a lander was dropped from the 2001 mission objectives. Under the present exploration plan, a 2009 opportunity for a precision landing demonstration exists. The entry vehicle for this potential mission is referred to as a Smart Lander.[6]

Had the 2001 lander mission been attempted, it would have represented the first autonomously directed entry into Mars by a lifting

Received 10 October 2002; revision received 1 August 2004; accepted for publication 1 February 2005.

*Aerospace Engineer, Aerothermodynamics Branch. Senior Member AIAA.
†Cooperative Education Student.
‡Aerospace Engineer, Space Access and Exploration Program Office. Associate Fellow AIAA.
§Aerospace Engineer, Lockheed Martin Engineering and Sciences Company.

vehicle using an atmospheric guidance algorithm for Mars.[7–10] In contrast to the nonlifting ballistic entries flown by Pathfinder and the Mars Polar Lander and the lifting entries flown by the Viking Landers,[11] the initial entry strategy for the 2001 Lander called for directional control of the entry vehicle lift vector through bank-angle modulation. Control of the lift vector was to be provided by reaction control jets. To expedite lander construction and minimize cost, the baseline conuration for the 2001 lander was leveraged from Pathfinder and the Mars Polar Lander designs, which consisted of a Viking heritage 70-deg spherically blunted cone with a conic afterbody.

Traditionally, such blunt axisymmetric shapes can produce lift by flying at incidence and are aerodynamically trimmed via a center-of-gravity offset. Because Pathfinder and the Mars Polar lander flew ballistic entries, these flight vehicles did not possess a nominal c.g. offset. Constrained by these previous designs (expedite lander construction/minimize tooling costs), structural and weight constraints of the proposed 2001 lander (which was to fly a lifting trajectory) did not permit the radial c.g. offset required for aerodynamic trim [at the desired lift-to-drag ratio (L/D)] that would normally be achieved through payload packaging trades or ballast mass. This required that alternative methods to provide aerodynamic trim be examined.[2]

This paper details an investigation designed to assess the aerodynamic feasibility of one such proposal; a single-body flap to trim the lander at angle of attack during hypersonic planetary entry. An inviscid flow solver was used to rapidly evaluate several flaps with the potential to provide sufficient trim capability to meet mission objectives. Experimental force and moment measurements are then compared to Navier–Stokes prediction.

An early Smart Lander concept using a flap to provide aerodynamic trim is shown in Fig. 1. Historically, the concept of a flap to provide aerodynamic trim on similar axisymmetric blunt capsule shapes can be found as early as 1961 and is reported in Ref. 12. As an alternative method to provide aerodynamic trim for the 2001 lander, the viability of the flap would be determined by its ability to provide similar or better aerodynamic performance across the Mach-number range relative to that achieved with an offset c.g. For future missions requiring precision landing (in which constraints for an offset c.g. are more relaxed), a flap can still serve as an attractive means for providing aerodynamic trim.

Fig. 1 Proposed Mars Smart Lander entry at Mars using flap to provide aerodynamic trim. (Photo courtesy of Bill Kluge, Langley Research Center.)

It was anticipated that entry of the Mars Surveyor Precision Lander into the atmosphere of Mars (continuum-flow regime) would produce maximum values of normal shock density ratio (ρ_2/ρ_∞) near 20. These high values of normal shock density ratio encountered in hypervelocity flight are produced from dissociation of atmospheric gases (because of high temperature effects) as they cross through the shock wave into the shock layer and are often referred to as real-gas effects. It is well recognized that the normal shock density ratio is one of the primary flight simulation parameters that govern the inviscid flow and aerodynamics of blunt bodies at hypersonic speeds.[13,14] Real-gas effects can impact the aerodynamics of a vehicle through changes in both the magnitude and distribution of surface pressure. During entry of blunt vehicles into the Martian atmosphere, values of normal shock density ratio are encountered that are significantly larger (two to three times) than those produced in conventional blowdown hypersonic wind tunnels using air or nitrogen as a test gas.[13]

Currently active conventional-type hypersonic blowdown tunnels are incapable of providing normal shock density ratios near 20. High-enthalpy impulse facilities, although capable, are not typically used from an aerodynamic screening perspective because of extremely short test times. The NASA Langley 20-Inch Mach 6 CF_4 Tunnel was developed to provide a unique alternative to high-enthalpy testing.[14,15] This conventional blowdown tunnel uses a test gas (tetrafluoromethane; CF_4) with a molecular weight three times that of air to generate a normal shock density ratio of 12, thereby simulating this particular aspect of a real gas. The simulation is achieved at moderate levels of enthalpy and without dissociation of the test gas. Based on the proposed entry trajectory of the 2001 Lander, the heavy gas tests in CF_4 simulate a Mach number of approximately 12 based on a normal shock density ratio of 12 in flight at Mars. An estimate of blunt-body aerodynamic effects attributed to a real gas can be obtained by synergistic testing in Mach 6 ideal air at a comparable Reynolds number.

The Langley 20-Inch Mach 6 Air and CF_4 Tunnels were used to assess the laminar aerodynamic characteristics of the Mars Surveyor 2001 Precision Lander using a flap to provide aerodynamic trim. Three flap sizes were tested at a freestream unit Reynolds number ranging from 0.03×10^6/ft to 2.3×10^6/ft (postshock Reynolds number based on body diameter of 2.637×10^3 to 92.350×10^3). The Mars Precision Lander model was tested at angles of attack from 0 to 23 deg with select data at 2-deg sideslip. Schlieren images provided details of the shock structure about the proposed entry configuration.

Experimental Methods

Model

The 3-in.-diam stainless-steel force and moment model is a 0.029-scale representation of the proposed Mars Surveyor 2001 Lander.[2] A dimensioned sketch of the baseline 2001 MSPL flight geometry is shown in Fig. 2. Drawing on the heritage of past planetary missions to Mars, the 2001 Lander forebody consists of a spherically blunted 70-deg half-angle cone with a truncated conical afterbody. The model was designed to accept multiple stainless-steel flaps (trim tabs). The flap hingeline was located downstream of the forebody maximum diameter (at the tangency point of the shoulder radius and conical afterbody). At this location, the individual flaps project radially outward, 90 deg from the longitudinal axis of symmetry. The model/balance was supported by a cylindrical steel rod (sting), which extended downstream from the model base. In addition, a thin-walled protective aluminum shroud extended over the balance and support sting. To determine the possible influence of the support system on aerodynamics, several runs were made with this aluminum shroud removed, which

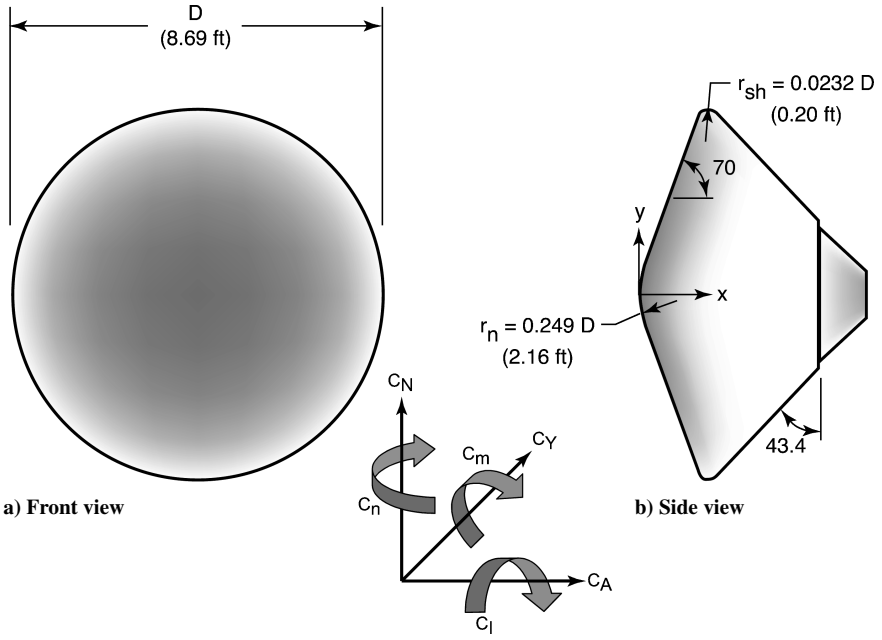

Fig. 2 Sketch of 2001 Mars Surveyor Precision Lander flight vehicle configuration.

Table 1 Model configurations

Configuration	L_{ref}, in.	S_{ref}, in.	b_{ref}, in.	$X_{\text{c.g.}}$, in.	$S_{\text{flap}}/S_{\text{forebody}}$
Baseline	3	7.07	3	0	——
Baseline + flap 1	3	7.07	3	0	0.0212
Baseline + flap 2	3	7.07	3	0	0.0398
Baseline + flap 3	3	7.07	3	0	0.0606

decreased the sting-to-forebody diameter ratio (d_s/d_f) from 0.40 to 0.17.

The size of the three candidate flaps examined in this experimental study was initially based on modified Newtonian predictions as discussed in Ref. 2 and subsequent inviscid computations provided by the Euler solver, FELISA (to be discussed in the Computational Methods section). Table 1 details the model/flap configurations that were tested and lists the reference values used to calculate the aerodynamic coefficients. The photographs in Fig. 3 illustrate the flap surface area relative to the forebody frontal area. The projected flap areas normalized to the forebody frontal area are also presented in Table 1.

Facility Descriptions

Tests were conducted in two facilities managed under the Langley Aerothermodynamic Laboratory (LAL). This complex presently consists of four hypersonic wind tunnels that represent a large fraction of the nation's conventional aerothermodynamic test capability.[16] Collectively, they provide a range of Mach number, unit Reynolds number, and normal shock density ratio. This range of hypersonic simulation parameters is caused, in part, by the use of two different test gases (air and tetraflouromethane), thereby making the facilities unique national assets. The LAL facilities are relatively small and economical to operate, hence ideally suited for fast-paced aerodynamic performance and aeroheating studies aimed at screening, assessing, optimizing, and benchmarking (when combined with computational fluid dynamics) advanced aerospace vehicle concepts and basic fundamental flow physics research.

20-Inch Mach 6 Air Tunnel

Heated, dried, and filtered air is used as the test gas. Typical calibrated operating conditions for the tunnel are stagnation pressures ranging from 30 to 500 psia; stagnation temperatures from 410 to 500°F; and freestream unit Reynolds numbers from 0.5×10^6 to 8×10^6/ft. A two-dimensional, contoured nozzle is used to provide nominal freestream Mach numbers from 5.8 to 6.1. The closed test section is 20.5×20 in.; the nozzle throat is 0.399×20.5 in. A bottom-mounted model injection system can insert models from a sheltered position to the tunnel centerline in less than 0.5 s. A detailed description of this facility can be found in Ref. 16.

Table 2 Nominal flow conditions

Re_∞/ft ($\times 10^6$)	$Re_{2,D}$	M_∞	Test gas	$P_{t,1}$, psi	$T_{t,1}$, °R	ρ_2/ρ_∞
0.66	26,425	5.8	Air	33	866	5.23
1.23	49,125	5.9	Air	64	879	5.24
2.33	92,350	5.9	Air	130	900	5.26
0.03	2,637	6.0	CF_4	119	1,305	12.0
0.11	10,935	5.8	CF_4	388	1,305	11.7
0.32	31,175	5.9	CF_4	1,069	1,296	11.8

20-Inch Mach 6 CF_4 Tunnel

Heated, dried, and filtered tetrafluoromethane (CF_4) is used as the test gas. Typical calibrated operating conditions for the tunnel are stagnation pressures ranging from 85 to 2000 psia, stagnation temperatures up to 840°F, and freestream unit Reynolds numbers from 0.01×10^6 to 0.41×10^6/ft. A contoured axisymmetric nozzle is used to provide nominal freestream Mach numbers from 5.9 to 6.2. The nozzle exit diameter is 20 in. with the flow exhausting into an open-jet test section; the nozzle throat diameter is 0.466 in. A bottom-mounted model injection system can inject models from a sheltered position to the tunnel centerline in less than 0.5 s. A detailed description of this facility can be found in Refs. 14 and 15.

Test Conditions and Setup

Nominal reservoir and corresponding freestream flow conditions for the MSPL test series are presented in Table 2. The freestream properties were determined from the measured reservoir pressure and temperature and the measured pitot pressure at the test section. Static pressure in the CF_4 test section that enclosed the open jet was monitored to assess the potential for contraction of the open-jet test core flow with time during any given run. Pitot and reservoir pressures were also measured in both facilities during each run to determine flow conditions and test times. The ratio of projected model frontal area to core flow cross-sectional area for the 0.029-scale model is approximately 0.28. Model angle of attack and sideslip were set to zero in the tunnel using a combination of

a) Baseline

c) Baseline plus flap 2

b) Baseline plus flap 1

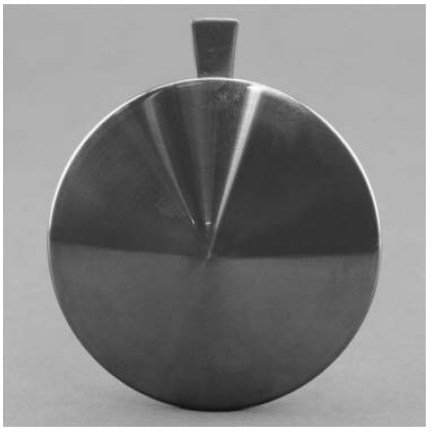

d) Baseline plus flap 3

Fig. 3 MSPL wind-tunnel model with flaps (see Table 1).

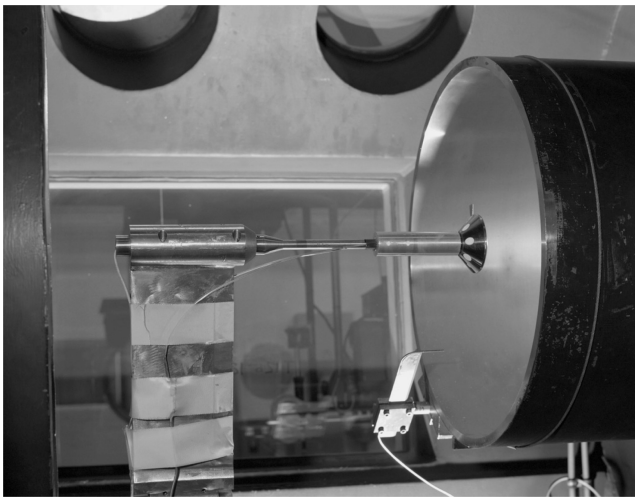

Fig. 4 The 0.029-scale MSPL aerodynamic model installed in the NASA LaRC 20-Inch Mach 6 CF_4 tunnel.

an inclinometer and a laser alignment system. A photograph of the MSPL model installation in the CF_4 tunnel is shown in Fig. 4.

Test Techniques

Force and Moment Measurements

Aerodynamic force and moment loads were measured using a sting-supported, six-component, water-cooled internal strain-gauge balance, Langley designation HN08B. The balance temperature was monitored using integrated water jacket thermocouples to ensure excessive thermal gradients did not develop during the run. An aluminum shroud was extended over the balance (see Fig. 5) to minimize heating to the balance from base flow impingement. The shroud attached to the sting and clearance was provided to avoid interference with the balance during model movement when aerodynamic forces were applied. In the CF_4 tunnel, the model was located approximately 0.5 in. downstream of the nozzle exit and laterally displaced 4 in. from the tunnel centerline to avoid small disturbances that are characteristic in axisymmetric nozzles. Limited tests made with the model on tunnel centerline did not indicate any measurable effect on the aerodynamic characteristics of the MSPL.

Schlieren Photography

Flow visualization in the form of schlieren was used to complement the surface temperature and heating measurements. The LaRC 20-Inch Mach 6 Air and CF_4 Tunnels are equipped with a pulsed white-light, Z-pattern, single-pass schlieren system with a field of view encompassing the entire test core. The light sources are pulsed for approximately 3 ms. Images were recorded on a high-resolution digital camera and enhanced with commercial software.

Base-Pressure Measurements

Base-pressure measurements were not obtained during the testing because of the combination of short run times and long base-pressure settling times. Previous experience in the CF_4 facility in which runs were performed at a fixed angle of attack have indicated that rather large diameter tubing is required to insure that base-pressure settling times are shorter than the available run time (20 s). Base-pressure measurements with the required tube diameter were not attempted so as to minimize the potential for additional interference effects that might be present because of the balance shroud. As a result, all axial-force coefficients C_A are reported as uncorrected for base pressure.

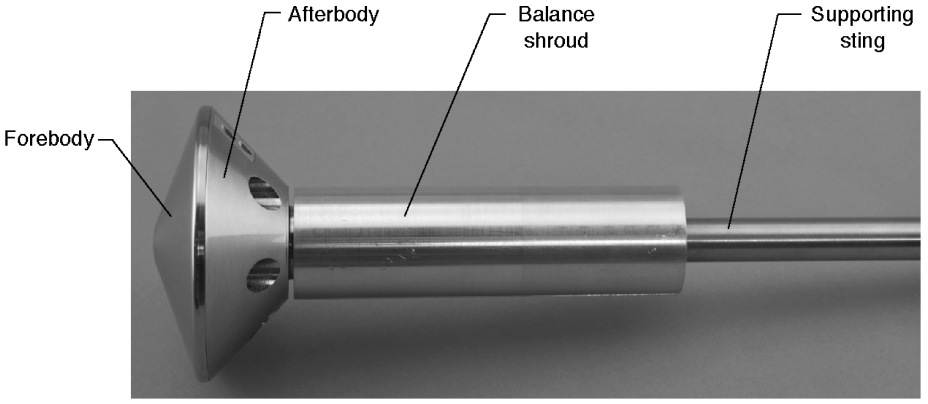

Fig. 5 MSPL aerodynamic model with balance shroud.

Table 3 Estimated force and moment coefficient uncertainties

Coefficient	Value
C_N	±0.008
C_A	±0.015
C_Y	±0.004
C_m	±0.003
C_n	±0.001
C_l	±0.001

Data Reduction and Uncertainty

A 16-bit analog-to-digital facility acquisition system was used to acquire flow condition data. Measured values of $P_{t,1}$ and $T_{t,1}$ are estimated to be accurate to within ±2%.

Aerodynamic data were obtained in an ascending pitch-pause manner during each run. Generally, two separate runs were required to complete a polar because of the short run time. The data were collected by an analog-to-digital data-acquisition system using an acquisition rate of 50 samples per second and averaged over a 1-s interval for each angle of attack (model held at fixed angle of attack for approximately 5 s). The raw data were transferred to a computer for data reduction and storage. During data reduction, corrections for weight tares, sting deflections, and balance interactions were made.

The force and moment data measured at the balance electrical center have been transferred to a moment reference center located at the forebody nose along the model x axis (see Fig. 2). The model outer mold lines were checked, and transfer distances were inferred from measurement by the NASA Langley Research Center surface verification laboratory. The balance electrical center was located 2.158 in. behind the configuration moment reference center. Table 1 lists the reference area and lengths used to calculate the aerodynamic coefficients.

Run-to-run repeatability (not shown) of the measured aerodynamic coefficients was generally better than 2%. The estimated uncertainty in the reported coefficients shown in Table 3 is based on 0.5% of the balance full-scale load for each component. Based on previous tests, this is considered a conservative estimate and generally will cover uncertainties caused by balance accuracy, data-acquisition accuracy, transfer distance measurement, and sting deflection.

Computational Methods

An unstructured inviscid flow solver (FELISA[17,18]) was used to provide a rapid assessment of the MSPL aerodynamics. The Langley aerothermodynamic upwind relaxation algorithm (LAURA)[19,20] was used to provide viscous laminar Navier–Stokes simulations of the MSPL aerodynamics at wind-tunnel conditions. Viscous (LAURA) and inviscid (FELISA) computations were made without an afterbody. The same thermodynamic properties for CF_4 were used in both codes. Limited Navier–Stokes predictions were made with the afterbody included to assess the influence of the base on the MSPL aerodynamics.

FELISA

The inviscid flow computations were performed using the unstructured grid software FELISA. This software package consists of a set of computer codes for unstructured grid generation[17] and the simulation of three-dimensional steady inviscid hypersonic flows[18] using unstructured tetrahedral grids. Surface triangulation and discretization of the computational domain using tetrahedral elements are accomplished with two separate codes. The grid used for the baseline MSPL configuration had 43,284 surface points and 902,024 interior points. The hypersonic flow solver has options for perfect-gas air, equilibrium air, CF_4, CO_2, and equilibrium Mars gases. The hypersonic flow solver with the CF_4 gas option was used for the present computations. Flow solutions were computed on a parallel computer. Surface pressures were integrated once every 50 steps during the iterations, and the aerodynamic loads were computed. The flow solution was assumed to have converged when these loads reached steady values. The contributions of the base to the aerodynamic loads were ignored (base pressure assumed to be equal to the freestream static pressure). More information on FELISA software can be found in Ref. 17. A description of the hypersonic flow solver can be found in Ref. 18.

LAURA

Viscous computations were performed by using the LAURA code. The LAURA code is a three-dimensional, finite volume solver that includes perfect-gas, equilibrium, and nonequilibrium chemistry models and can be used to solve the inviscid, thin-layer Navier–Stokes or full Navier–Stokes equations. For the current study, the thin-layer Navier–Stokes equations were solved using the CF_4 gas option. Freestream conditions for the LAURA wind-tunnel computations were set to the freestream operating conditions of the test, and no-slip conditions were applied at the model wall. A single-block, singularity-free grid topology was employed. The majority of solutions were computed on a forebody only grid containing $37 \times 40 \times 32$ cells (in the streamwise, circumferential, and body-normal directions, respectively), which included the forward face of the flap. Limited computations were made with an afterbody included to assess the influence of the base on the MSPL aerodynamics. For all solutions, grid adaptation was performed to align the bow shock with the grid and produced nominal wall cell Reynolds numbers on the order of one.

A grid-resolution study was performed for the configuration with the largest flap. First, the density of the cells in the normal direction was increased beyond the 32 cells in the standard grid. Three solutions were computed for 48, 64, and 96 cells, respectively. Additionally, three solutions for the largest flap were computed on a grid with a much finer surface mesh (148×112 cells) for 32, 64, and 96 cells, respectively, in the normal direction.

Results and Discussion

From an experimental viewpoint, the MSPL aerodynamic flap feasibility study conducted in the $M_\infty = 6\,CF_4$ tunnel was initially desirable from the perspective of testing in a gas with a high normal shock density ratio and a corresponding low ratio of specific heats γ as is encountered in hypervelocity flight. In addition, the facility provides the best opportunity from which to maintain a laminar flow because it operates at relatively low Reynolds numbers. More important, the shuttle orbiter first flight experience has underscored the importance of quantifying real-gas effects. As detailed in Ref. 21, the shuttle experienced a significant nose-up pitching-moment increment relative to preflight predictions resulting in body-flap deflections of twice the amount necessary to achieve trimmed flight. This phenomenon was later accurately simulated in the Langley CF_4 tunnel and was coupled with computational methods to provide a high degree of confidence in estimating hypersonic entry aerodynamics.[21] It is commonly recognized today that the primary effect of a real gas on aerodynamics is to lower the specific heat ratio γ within the shock layer, which in turn will produce a greater degree of flow compression and expansion relative to a perfect gas. Thus, compression surfaces (such as flaps) will have a correspondingly higher surface pressure. Because of the presence of a control surface near the rapidly expanding flow near the MSPL shoulder, aerodynamic real-gas simulation testing (similar to that conducted on the Viking lander and shuttle orbiter postflight) were performed.

From a computational aerodynamic screening perspective, FELISA provided a rapid assessment of the viability of a flap to provide aerodynamic trim. For the MSPL, a target trimmed L/D of at least 0.18 was required to provide adequate margins for a precision landing and was preferred based on Viking flight experience. I Aerodynamic predictions at wind-tunnel conditions provided by FELISA (Figs. 6a and 6b) indicated that a properly sized flap could provide sufficient aerodynamic trim at the required L/D.

The inviscid results from FELISA would not capture viscous effects such as skin friction and/or flow separation. Because skin friction over a forebody such as the MSPL for hypersonic freestream conditions at sufficiently high Reynolds number is negligible and afterbody contributions to aero are minimal, inviscid prediction should capture the overall aerodynamics (provided viscous effects on the MSPL flap are minimal).

Performance of the three flaps from the experimental heavy gas simulation tests relative to the measured baseline longitudinal aerodynamics (C_A, C_m, C_N, and L/D) of the MSPL at $M_\infty = 6\,CF_4$, $\rho_2/\rho_\infty = 12$ and $Re_{2D} = 0.03 \times 10^6$ is summarized in Figs. 7a–7d. Because the baseline shape is axisymmetric (with no flap), it trims at $\alpha = 0$ deg with an $L/D = 0$. As anticipated, the primary effect of the flaps was to change the MSPL trim angle of attack. At wind-tunnel conditions, a flap surface area approximately 6% of the forebody frontal area (flap 3) was shown to trim the MSPL near $\alpha = 11.5$ deg (Fig. 7b) at the desired L/D value of 0.18 (Fig. 7d). In comparison, Viking flight experience indicated the lander trimmed near 11-deg angle of attack (via a c.g. offset) during its entry at Mars.[22] The addition of the flaps on the MSPL did produce measurable increases in axial force (Fig. 7a) but was found to have no measurable effect on L/D performance (because L and D derived primarily from C_A for a blunt planetary configuration).

The effect of normal shock density ratio on laminar MSPL pitching-moment coefficient measurements obtained with the baseline and the baseline with the largest flap (flap 3) in air and CF_4 at identical Mach and Reynolds numbers is shown in Figs. 8a and 8b. The pitching-moment measurements made with the largest flap (Fig. 8b) suggest favorable real-gas effects at trim conditions; MSPL heavy gas simulation tests indicated a trimmed condition at 11.5 deg in contrast to 8.5 deg measured in air. The data indicate greater pitching-moment stability (more negative slope) than measured in air for $\alpha > 10$ deg. The corresponding laminar MSPL baseline (no flap; Fig. 8a) measurements obtained in air and CF_4 at identical Mach and Reynolds numbers exhibited the same stabilizing effect in CF_4 on pitching moment and were consistent with ground based trends measured for viking.[23] The crossover in pitching moment between the present air and CF_4 tests is consistent with Viking test experience.

No attempt was made in this screening study to optimize flap trim effectiveness through flap shape, orientation, or attachment location parametrics. In the context of the more mature MSPL designs, the flap was considered to be deployable retrofit as packaging a fixed control surface within the diameter of the launch vehicle shroud was unlikely. In the conceptual stages of this study, it was felt that the most effective location for the flap would be at or near the vehicle shoulder where the moment arm for the flap pressure loading is greatest. The deployable flap hingeline was located downstream of the forebody maximum diameter in a potentially more benign heating environment. In this position, the shadowed region in front of the flap was expected to produce a local flow separation.[2] Subsequent flow reattachment on the flap would result in an embedded shock. If a fixed flap were permissible, a simple surface extension beyond the conical forebody, such as that investigated in Ref. 12, might prove beneficial. This would eliminate the embedded shock system, thereby minimizing flap effectiveness sensitivity to Mach number, Reynolds number, and density ratio and avoid heating increases[24] caused by flow reattachment on the flap. These benefits would be weighted against the reduced flap pressure loading (and resultant requirement to increase flap size) in the absence of an embedded shock system.

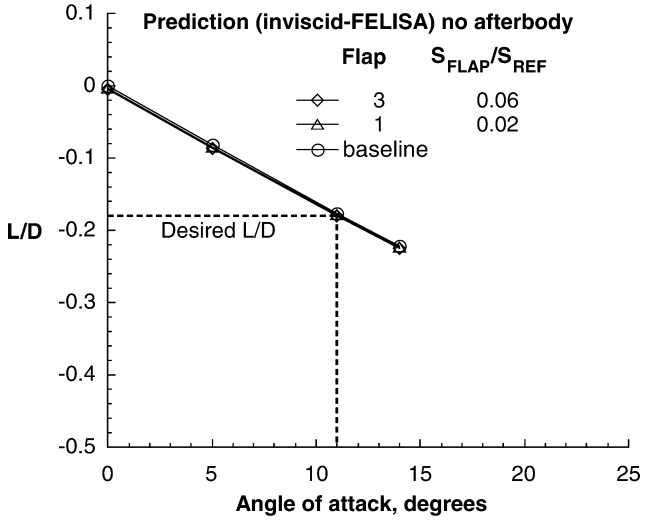

a) Lift-to-drag ratio

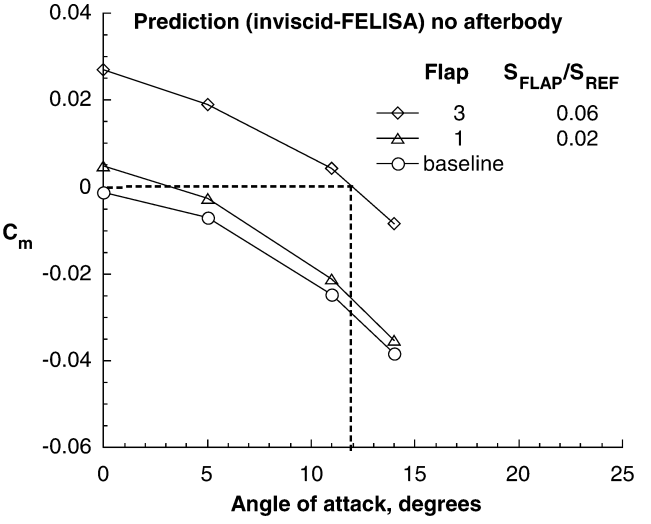

b) Pitching-moment coefficient

Fig. 6 Inviscid prediction of MSPL longitudinal aerodynamics provided by FELISA: $M_\infty = 6$, CF_4, $Re_{2D} = 0.03 \times 10^6$, and $\rho_2/\rho_\infty = 11.7$.

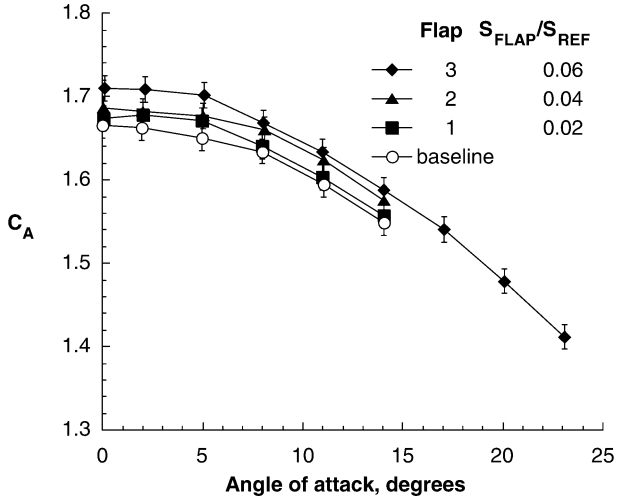

a) Axial-force coefficient

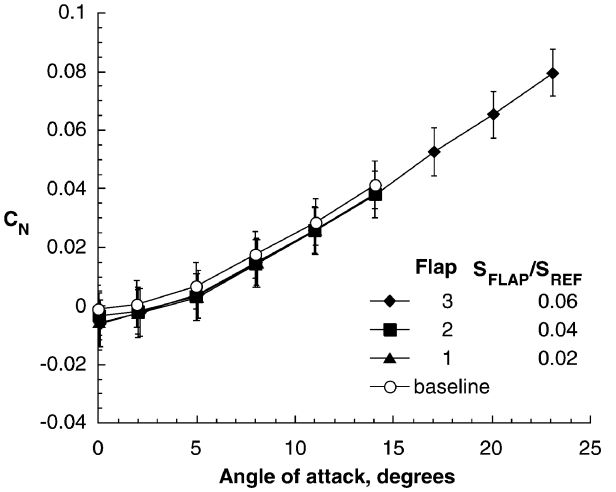

c) Normal-force coefficient

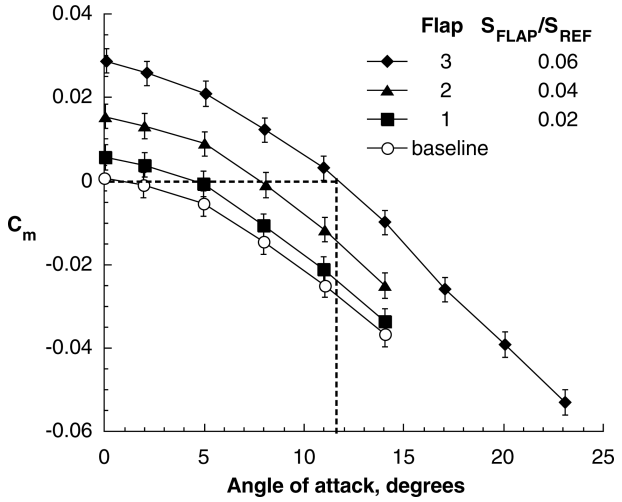

b) Pitching-moment coefficient

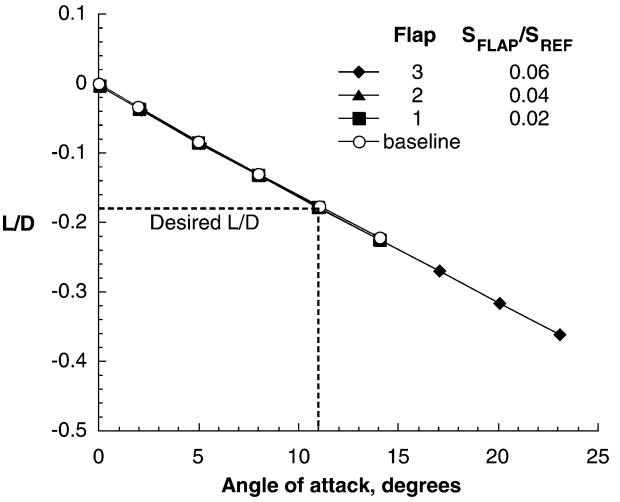

d) Lift-to-drag ratio

Fig. 7 Effect of flap size on MSPL longitudinal aerodynamics: $M_\infty = 6$, CF_4, $Re_{2D} = 0.03 \times 10^6$, and $\rho_2/\rho_\infty = 11.7$.

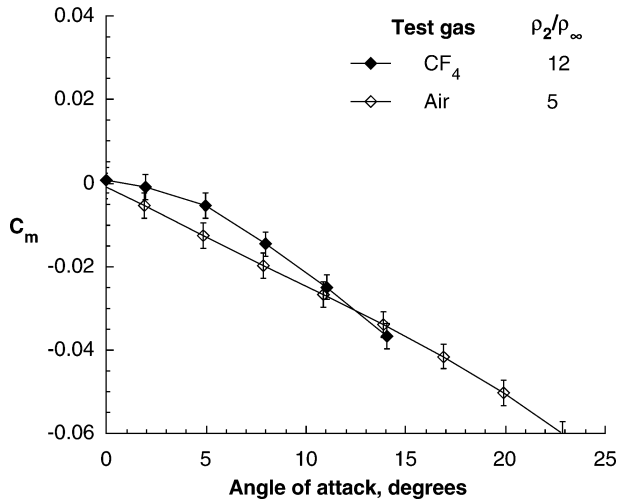

a) Baseline

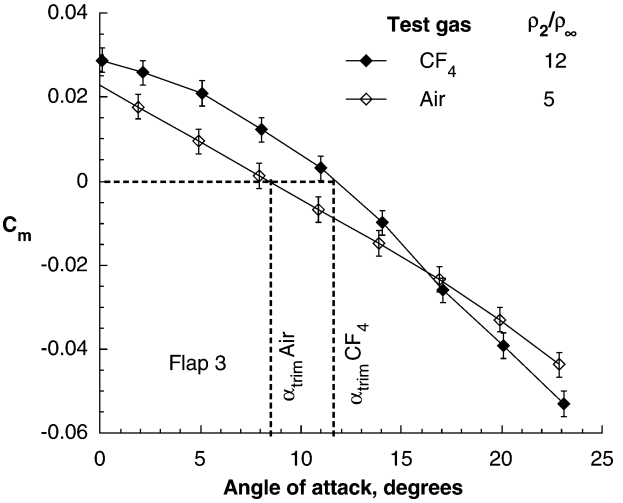

b) Baseline plus flap 3

Fig. 8 Effect of normal shock density ratio on MSPL pitching-moment coefficient: $M_\infty = 6$ and $Re_{2D} = 0.03 \times 10^6$.

Figures 9–12 show the comparisons of the measured longitudinal aerodynamics (C_A, C_m, C_N, and L/D) of the MSPL at $M_\infty = 6$ CF_4, $\rho_2/\rho_\infty = 12$, and $Re_{2D} = 0.03 \times 10^6$ to viscous predictions from LAURA at $\alpha = 0$ and 11 deg. Even with the afterbody excluded from the computations, the predicted pitching-moment and normal-force coefficients from LAURA were within the uncertainty of the measurement. Axial-force coefficient prediction was generally 1 to 4% lower than measurement, and thus was, in general, outside the lower limit of the estimated uncertainty. A grid-resolution study was performed on the baseline configuration with flap 3. An increase in wall normal cells from 32 to 96 produced a small increase (0.7%) in the axial aerodynamic coefficient (Fig. 12a). The corresponding comparisons of predicted pitching-moment and normal-force coefficients for this grid resolution study (Figs. 12b and 12c) were virtually indistinguishable. For aerodynamic screening purposes, this suggests that the impact of the embedded shock near the flap was adequately resolved with 32 cells in the normal direction.

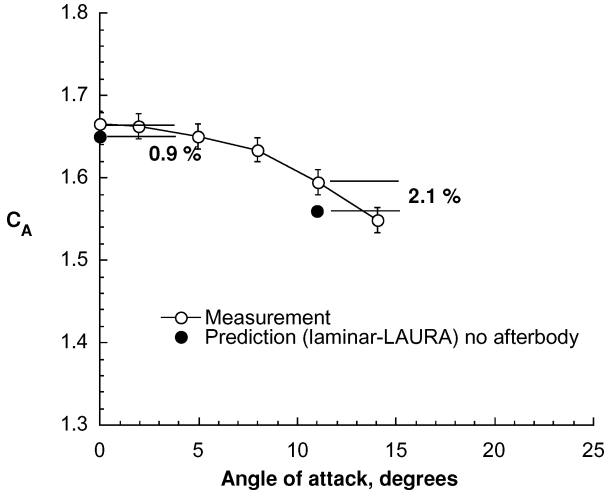

a) Axial-force coefficient

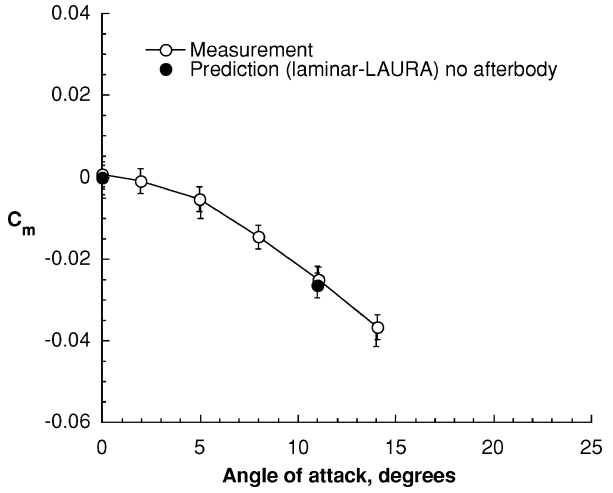

b) Pitching-moment coefficient

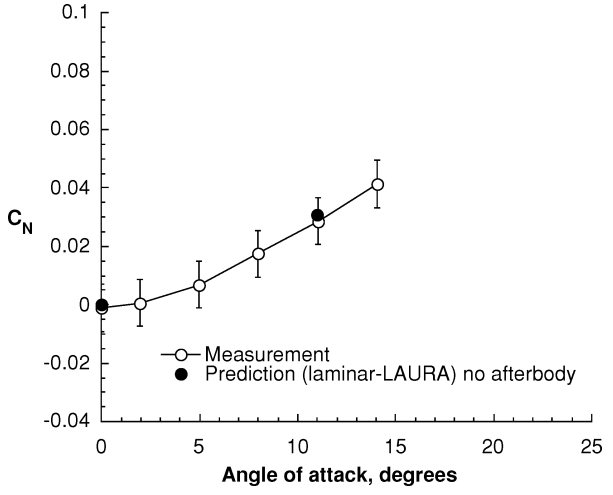

c) Normal-force coefficient

Fig. 9 Comparison of baseline MSPL longitudinal aerodynamics with prediction: $M_\infty = 6$, CF_4, $Re_{2D} = 0.03 \times 10^6$, and $\rho_2/\rho_\infty = 11.7$.

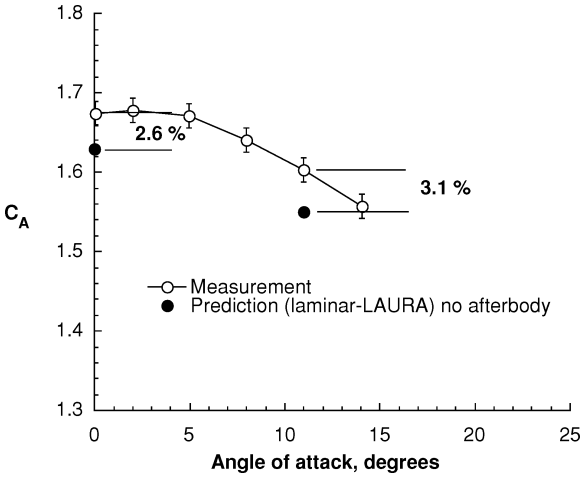

a) Axial-force coefficient

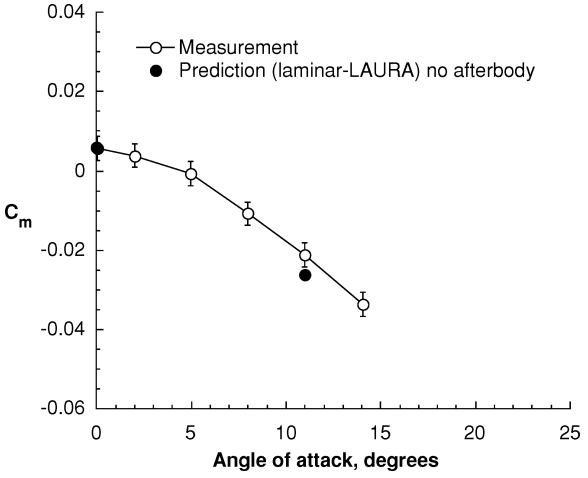

b) Pitching-moment coefficient

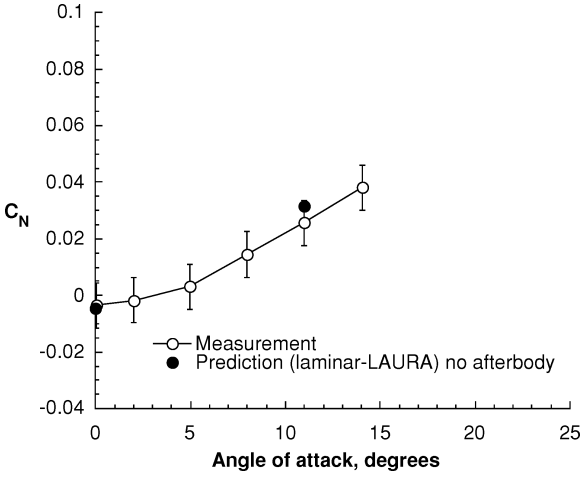

c) Normal-force coefficient

Fig. 10 Comparison of baseline + flap 1 MSPL longitudinal aerodynamics with prediction: $M_\infty = 6$, CF_4, $Re_{2D} = 0.03 \times 10^6$, and $\rho_2/\rho_\infty = 11.7$.

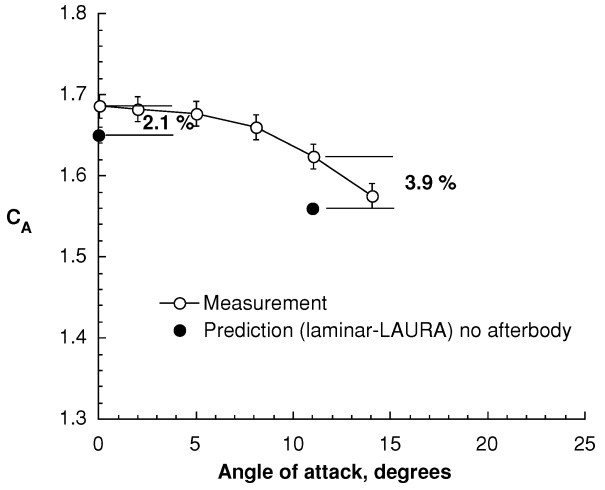

a) Axial-force coefficient

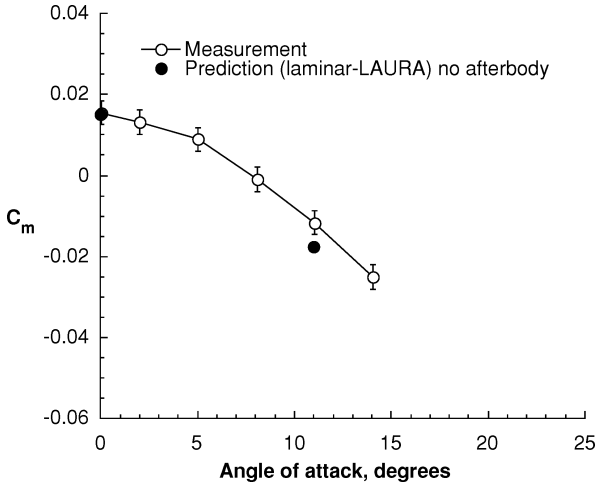

b) Pitching-moment coefficient

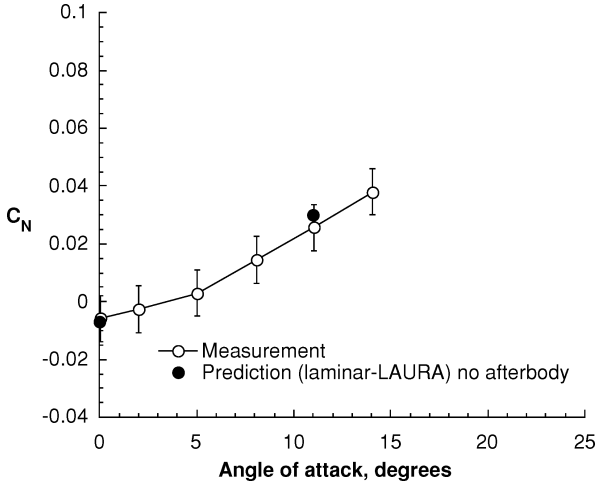

c) Normal-force coefficient

Fig. 11 Comparison of baseline + flap 2 MSPL longitudinal aerodynamics with prediction: $M_\infty = 6$, CF_4, $Re_{2D} = 0.03 \times 10^6$, and $\rho_2/\rho_\infty = 11.7$.

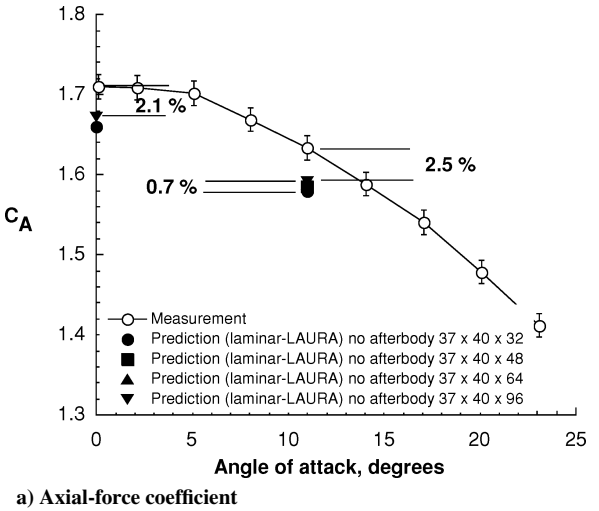

a) Axial-force coefficient

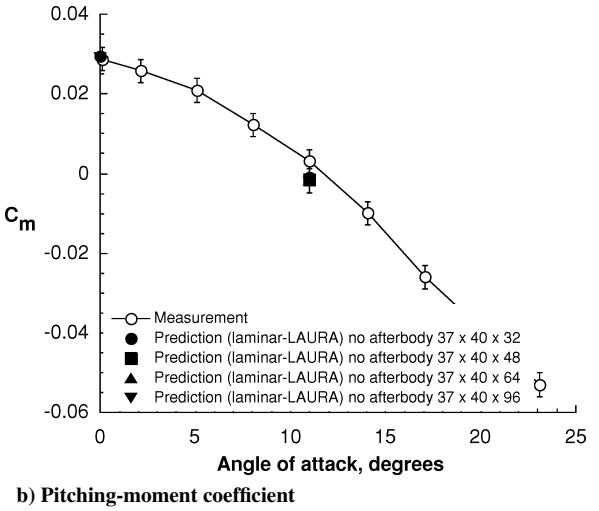

b) Pitching-moment coefficient

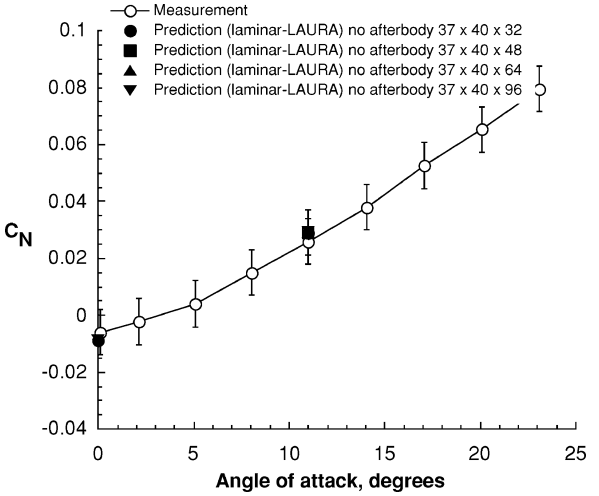

c) Normal-force coefficient

Fig. 12 Comparison of baseline + flap 3 MSPL longitudinal aerodynamics with prediction: $M_\infty = 6$, CF_4, $Re_{2D} = 0.03 \times 10^6$, and $\rho_2/\rho_\infty = 11.7$.

Outside the context of the model support sting, the influence of the base heat shield (or afterbody) on MSPL hypersonic aerodynamics was expected to be minimal. Previous blunt-body testing[25] in the CF_4 tunnel with an afterbody attached and removed (a model support sting was still present) indicated no measurable effect on longitudinal aerodynamics. Computational predictions made with LAURA on the MSPL baseline configuration with and without an afterbody are shown in Fig. 13. At $\alpha = 0$ deg, the presence of an afterbody increased C_A by approximately 0.02 and brought the difference between the predicted axial-force coefficient and measurement to less than 1%. Comparing the magnitude of the computed base-pressure correction (by including the afterbody) to those estimated from an engineering formula[26]:

$$\Delta C_{\mathrm{A,\ base\ correction}} = \left(1/M_\infty^2\right) - \left(0.57/M_\infty^4\right) \qquad (1)$$

indicated the LAURA corrections (with/without afterbody) to be 25% smaller. The increment in C_A and the differences in the

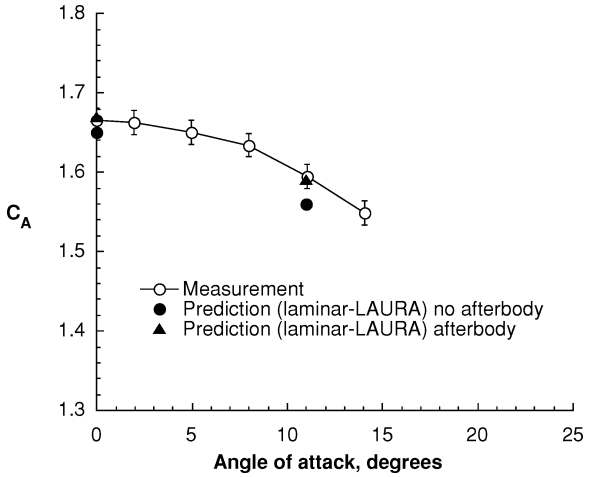

a) Axial-force coefficient

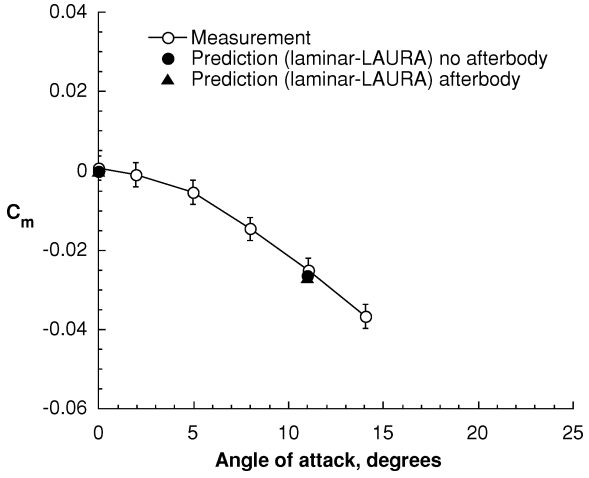

b) Pitching-moment coefficient

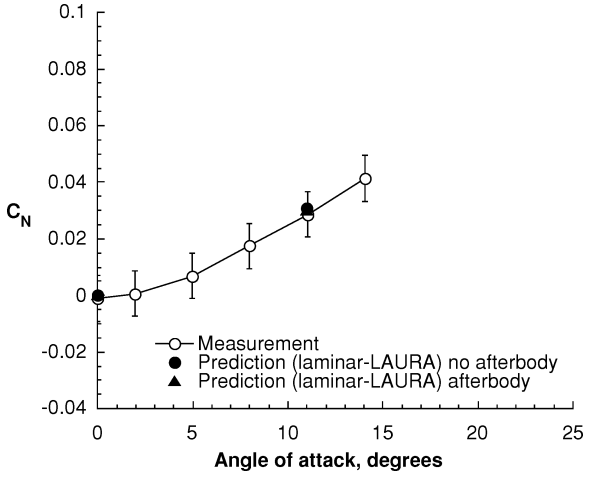

c) Normal-force coefficient

Fig. 13 Effect of afterbody on predicted baseline MSPL longitudinal aerodynamics and comparison to measurement: $M_\infty = 6$, CF_4, $Re_{2D} = 0.03 \times 10^6$, and $\rho_2/\rho_\infty = 11.7$.

magnitude of the correction with and without an afterbody are consistent with previous hypersonic LAURA blunt-body analysis[27] and indicated a viscous shear contribution from the afterbody. The corresponding comparisons of predicted pitching-moment and normal-force coefficients in the presence and absence of an afterbody show the results are virtually indistinguishable.

Because of its potentially more intrusive geometry, it is generally recognized that the presence of a model support sting can have a greater effect on the base flow characteristics of a blunt body in hypersonic flow. Experimental quantification of the effect with and without a support sting for this test series was not made. However, a limited data set was taken to assess the sensitivity of the MSPL aerodynamic drag measurements to the potential effects of a cylindrical model support sting for sting-to-model forebody diameter ratios of 0.40 (balance shroud attached; see Fig. 5) and 0.17 (balance shroud removed). At $Re_{2D} = 0.03 \times 10^6$, $M_\infty = 6\,CF_4$, and $\alpha = 0$ deg, no measurable aerodynamic effect from the differences

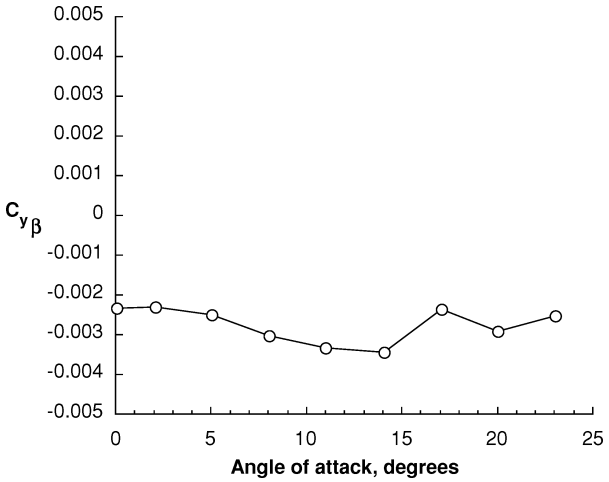

a) Side-force derivative

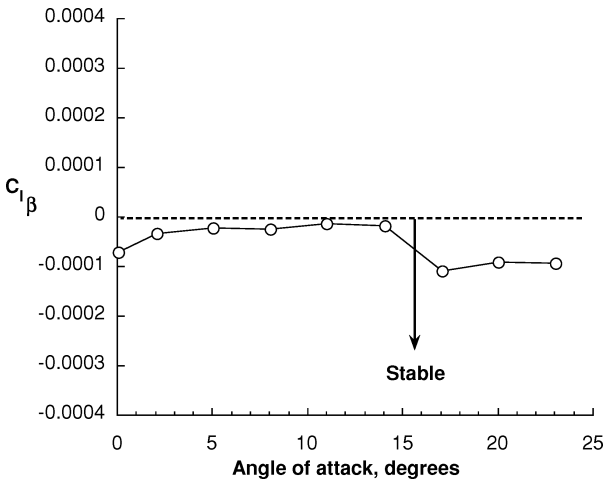

b) Rolling-moment derivative

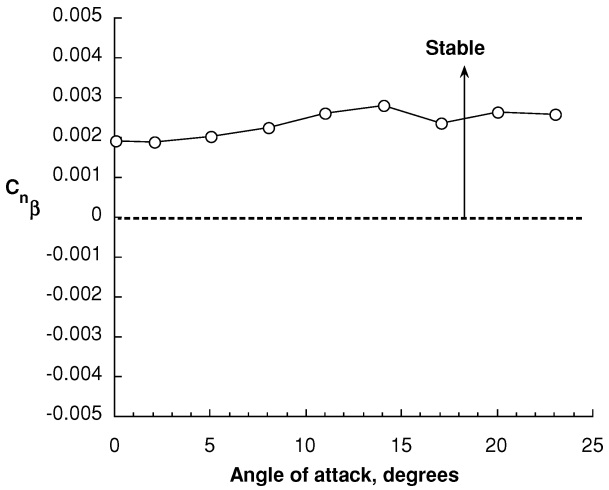

c) Yawing-moment derivative

Fig. 14 MSPL lateral/directional aerodynamics: $M_\infty = 6$, CF_4, $Re_{2D} = 0.03 \times 10^6$, $\rho_2/\rho_\infty = 11.7$, and $\beta = \pm 2$ deg.

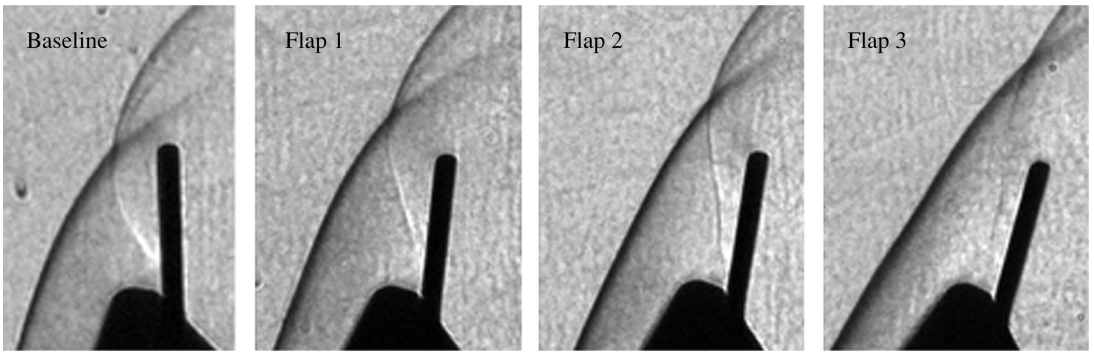

Fig. 15 Effect of flap size on MSPL shock shape and interaction: $M_\infty = 6$, CF_4, $\rho_2/\rho_\infty = 11.7$, $Re_{2D} = 0.03 \times 10^6$, and $\alpha = 11$ deg.

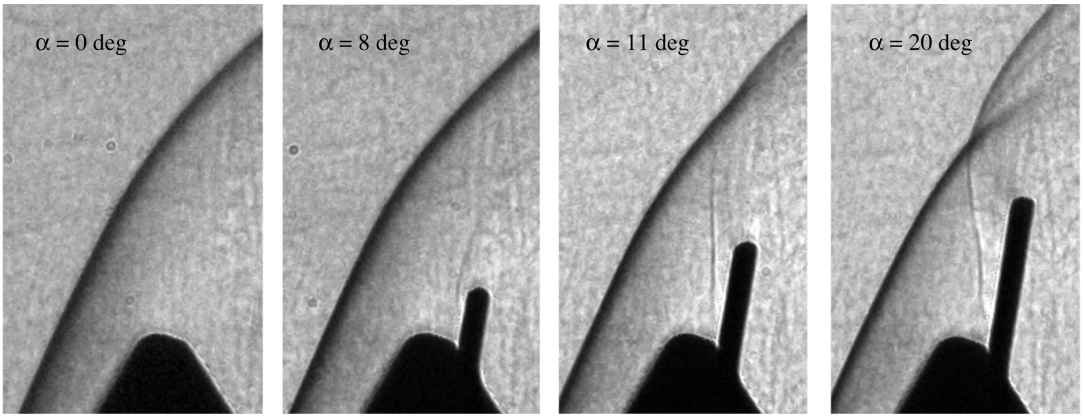

Fig. 16 Effect of angle of attack on MSPL shock shape and interaction: $M_\infty = 6$, CF_4, $\rho_2/\rho_\infty = 11.7$, $Re_{2D} = 0.03 \times 10^6$, and flap 3.

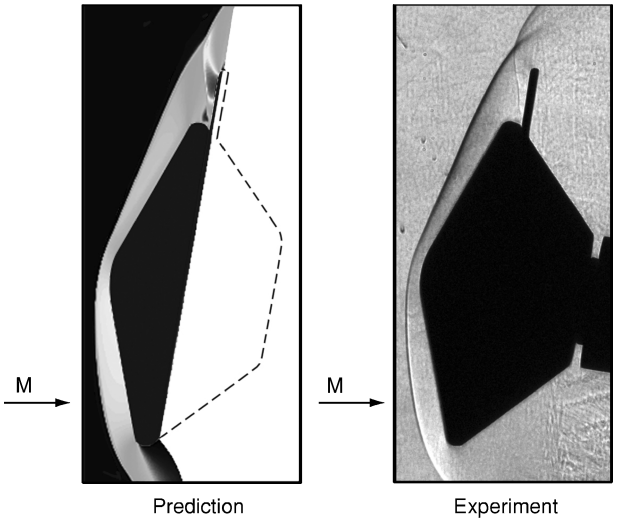

Fig. 17 Comparison of predicted MSPL density contours with measured schlieren image: $M_\infty = 6$, CF_4, $\rho_2/\rho_\infty = 11.7$, $Re_{2D} = 0.03 \times 10^6$, $\alpha = 11$ deg, and flap 3.

in model support was observed (not shown). Measurements at incidence were not attempted as flow impingement on the unprotected balance (shroud removed) was anticipated.

Because the MSPL baseline configuration was symmetric, it was anticipated that the vehicle would be laterally/directionally stable at sideslip angles anticipated for flight ($\beta < 2$ deg). A limited experimental assessment of static lateral/directional aerodynamics ($C_{y,\beta}$, $C_{l,\beta}$, and $C_{n,\beta}$) of the MSPL (configured with flap 3) at a side slip angle of 2 deg indicated the lander was statically stable as shown in Fig. 14 through the test range of angle of attack.

Schlieren images for the MSPL baseline and baseline plus flaps (at $M_\infty = 6\,CF_4$, $Re_{2D} = 0.03 \times 10^6$) are presented in Fig. 15, for $\alpha = 11$ deg. In the sequence of images, an embedded shock associated with the flow expansion and separation around the aerobrake shoulder, and subsequent reattachment and recompression, is evident for all three flaps. The flap aerodynamic effectiveness in flight would be dictated by the strength of this embedded shock. Further quantification of real-gas effects and Mach number on flap pressure loading would be essential in determining the viability of any flap to provide aerodynamic trim at the appropriate values of L/D for the duration of its atmospheric trajectory.

Schlieren images for the MSPL baseline with flap 3 (in $M_\infty = 6\,CF_4$, $Re_{2D} = 0.03 \times 10^6$) are presented in Fig. 16, for a range of angle of attack ($0 < \alpha < +20$ deg). As expected, the embedded shock system persists over the range of angle of attack. Comparisons of the measured shock shape of the MSPL baseline +flap 3 at $\alpha = 11$ deg with a thin-layer Navier–Stokes prediction (for the $148 \times 112 \times 96$ grid) are presented in Fig. 17. The predicted bow shock standoff distance and the spatial location and shape of the embedded shock associated with the flap (inferred from the computational density contour mapping) were in excellent agreement (within 2%) with measurement.

Conclusions

The Langley 20-Inch Mach 6 Air and CF_4 Tunnels were used to assess the aerodynamic characteristics of the Mars Surveyor 2001 Precision Lander using a base flap to provide aerodynamic trim. Three flap sizes were evaluated over a range of freestream unit Reynolds number from 0.03×10^6 to 2.23×10^6 at a nominal freestream Mach number of 6. The model was tested at angles of attack from 0 deg up to 23 deg with select data at 2-deg sideslip. Based upon the proposed entry trajectory of the MSPL, the heavy gas tests in CF_4 simulate a Mach number of approximately 12 based on a normal shock density ratio of 12 in flight at Mars. The resulting laminar aerodynamic measurements obtained in air and CF_4 at comparable Mach and Reynolds number indicate favorable real-gas effects at trim conditions. The CF_4 data indicate greater pitching-moment stability than measured in air for $\alpha > 10$ deg; MSPL heavy gas simulation tests with the largest flap indicated a trimmed condition at

11.5-deg angle of attack in contrast to 8.5 deg measured in perfect-gas air. A limited assessment of static lateral/directional aerodynamics at a sideslip angle of 2 deg indicated the lander was stable through the test range of angle of attack.

Inviscid prediction with an unstructured hypersonic flow solver (FELISA) provided a rapid assessment on the viability of a flap to provide aerodynamic trim at the desired L/D. Longitudinal aerodynamic coefficients predicted with a viscous solver (LAURA) were generally within the estimated measurement uncertainty. Computations that included the afterbody brought the difference between the predicted axial force coefficient and measurement to less than 1%.

When traditional means of providing aerodynamic trim for this blunt class of planetary entry vehicle are not possible (offset c.g.), a single flap can provide similar aerodynamic performance. Whether fixed or deployable, the viability of the flap to a provide trim capability would reside in trade studies to determine mass/ballast penalties associated with flap attachment or deployment hardware and additional control surface thermal protection requirements.

Acknowledgments

Without the assistance of the following individuals, this work would not have been possible: Ed Carden, Harry Stotler, Mike Fleck, Dave Fahringer, Dave Roberts, Alan Scheidegger, Ed Covington, and Tom Burns for model design/fabrication/instrumentation/surface inspection support; Grace Gleason, John Ellis, Roland Hatten, Melanie Lawhorne, Harry Stotler, Christal Kellam, and Al Garner for wind-tunnel support; Sheila Wright and Bert Senter for data-acquisition assistance; Robert Braun, Robert Mitcheltree, and Ken Sutton for technical discussions; and Richard Wheless for documentation assistance. The authors gratefully acknowledge their contributions and behind-the-scenes work.

References

[1]Lockwood, M. K., Powell, R. W., Graves, C. A., and Carman, G. L., "Entry System Design Considerations for Mars Landers," American Astronautical Society, Paper 01-023, Jan. 2001.

[2]Braun, R. D., Powell, R. W., Cheatwood, F. M., Spencer, D. A., and Mase, R. A., "The Mars Surveyor 2001 Lander: A First Step Towards Precision Landing," International Astronautical Federation, Paper 98-Q.3.03, Sept. 1998.

[3]Smith, B. A., "Lander Development Paced By Mars Science Results," *Aviation Week and Space Technology*, Vol. 152, No. 26, 2000, p. 63.

[4]Pieri, D., "Rebuilding the U.S. Mars Exploration Program," *Launchspace*, Vol. 5, No. 6, 2000, p. 27.

[5]Smith, B. A., "NASA Weighs Mission Options," *Aviation Week and Space Technology*, Vol. 153, No. 24, 2000, p. 54.

[6]Lockwood, M. K., Powell, R. W., Sutton, K., Prabhu, R. K., Graves, C. A., Epp, C. D., and Carman, G. L., "Entry Configurations and Performance Comparisons for Mars Smart Lander," *Journal of Spacecraft and Rockets*, Vol. 43, No. 2, 2006, pp. 258–269; also AIAA Paper 2002-4407, Aug. 2002.

[7]Striepe, S. A., Queen, E. M., Powell, R. W., Aguirre, J. T., Sachi, L. A., and Lyons, D. T., "An Atmospheric Guidance Algorithm Testbed for the Mars Surveyor Program 2001 Orbiter and Lander," AIAA Paper 98-4569, Aug. 1998.

[8]Carman, G., Ives, D., and Geller, D., "Apollo-Derived Mars Precision Lander Guidance," AIAA Paper 98-4570, Aug. 1998.

[9]Tu, K.-Y., Munir, M. S., Mease, K. D., and Bayard, D. S., "Drag-Based Predictive Tracking Guidance for Mars Precision Landing," *Journal of Guidance, Control, and Dynamics*, Vol. 23, No. 4, 2000, pp. 620–628.

[10]Powell, R. W., "Numerical Roll Reversal Predictor-Corrector Aerocapture and Precision Landing Guidance Algorithms for the Mars Surveyor Program 2001 Missions," AIAA Paper 98-4574, Aug. 1998.

[11]Blanchard, R. C., Wilmoth, R. G., and Moss, J. N., "Aerodynamic Flight Measurements and Rarefied-Flow Simulations of Mars Entry Vehicles," *Journal of Spacecraft and Rockets*, Vol. 34, No. 5, 1997, pp. 687–690.

[12]Sammonds, R. I., and Dickey, R. R., "Effectiveness of Several Control Arrangements on a Mercury-Type Capsule," NASA TM X-579, Oct. 1961.

[13]Jones, R. A., and Hunt, J. L., "Use of Tetrafluoromethane to Simulate Real-Gas Effects on the Hypersonic Aerodynamics of Blunt Bodies," NASA TR R-312, June 1969.

[14]Midden, R. E., and Miller, C. G., III, "Description and Calibration of the Langley Hypersonic CF_4 Tunnel: A Facility for Simulating Low Gamma Flow as Occurs for a Real Gas," NASA TP 2384, March 1985.

[15]Micol, J. M., Midden, R. E., and Miller, C. G., III, "Langley 20-Inch Hypersonic CF_4 Tunnel: A Facility for Simulating Real Gas Effects," AIAA Paper 92-3939, July 1992.

[16]Miller, C. G., III, "Langley Hypersonic Aerodynamic/Aerothermodynamic Testing Capabilities—Present and Future," AIAA Paper 90-1376, June 1990.

[17]Peiro, J., Peraire, J., and Morgan, K., "FELISA System Reference Manual and Users Guide," Univ. College of Swansea, Tech. Report, Swansea, Wales, U.K., Dec. 1993; also NASA CP3291, May 1995.

[18]Bibb, K. L., Peraire, J., and Riley, C. J., "Hypersonic Flow Computations on Unstructured Meshes," AIAA Paper 97-0625, Jan. 1997.

[19]Gnoffo, P. A., "An Upwind-Biased, Point-Implicit Relaxation Algorithm for Viscous Compressible Perfect Gas Flows," NASA TP 2953, Feb. 1990.

[20]Cheatwood, F. M., and Gnoffo, P. A., "User's Manual for the Langley Aerothermodynamic Upwind Relaxation Algorithm (LAURA)," NASA TM 4674, April 1996.

[21]Brauckmann, G. J., Paulson, J. W., and Weilmuenster, J. K., "Experimental and Computational Analysis of the Space Shuttle Orbiter Hypersonic Pitch-Up Anomaly," AIAA Paper 94-0632, Jan. 1994.

[22]Blanchard, R. C., Wilmoth, R. G., and Moss, J. N., "Aerodynamic Flight Measurements and Rarefied-Flow Simulations of Mars Entry Vehicles," *Journal of Spacecraft and Rockets*, Vol. 34, No. 5, 1997, pp. 687–690.

[23]Hunt, J. L., Jones, R. A., and Midden, R. E., "Simulation of Real-Gas Effects for Mars Entry," *Journal of Spacecraft and Rockets*, Vol. 11, No. 1, 1974, pp. 62–64.

[24]Liechty, D. S., and Hollis, B. R., "Control Surface and Afterbody Experimental Aeroheating for a Proposed Mars Smart Lander Aeroshell," AIAA Paper 2002-4506, Aug. 2002.

[25]Wells, W. L., "Measured and Predicted Aerodynamic Coefficients and Shock Shapes for Aeroassist Flight Experiment (AFE) Configuration," NASA TP-2956, Jan. 1990.

[26]Bonner, E., Cleaver, W., and Dunn, K., "Aerodynamic Preliminary Analysis System II. Part I-Theory," NASA CR-182076, April 1991.

[27]Wood, W. A., Gnoffo, P. A., and Rault, D. F., "Aerodynamic Anaylis of Commercial Experiment Transporter Re-Entry Capsule," *Journal of Spacecraft and Rockets*, Vol. 33, No. 5, 1996, pp. 643–646.

M. K. Lockwood
Guest Editor